https://doi.org/10.5194/essd-2026-161
Preprint. Discussion started: 24 March 2026

Open Access Earth System Science Data Discussions

Mapping Plant Growth Index (PGI) over Australia from 1990 to 2024

Renata Retkute[1], Allan Spessa[2], David Hunter[2], Christopher A. Gilligan[1]

[1] Epidemiology and Modelling Group, Department of Plant Sciences, University of Cambridge, Downing Street, Cambridge CB2 3EA, UK

[2] The Australian Plague Locust Commission, Unit 7, 50 Collie Street, Fyshwick ACT 2609, Australia

Correspondence to: Renata Retkute (rr614@cam.ac.uk)

Abstract. Australia spans nearly the full spectrum of global bioclimatic zones, from tropical savannas to arid deserts and alpine environments. Understanding how climate constrains vegetation growth across this gradient is essential for interpreting ecosystem dynamics and informing land-management decisions. We introduce a Plant Growth Index (PGI), a continental-scale metric derived from meteorological data from the Bureau of Meteorology Atmospheric high-resolution Regional Reanalysis for Australia (BARRA-R), European Space Agency (ESA) Plant Functional Type (PFT) layers, and C_3/C_4 grass fractions estimated from NASA Moderate Resolution Imaging Spectroradiometer (MODIS) enhanced vegetation index (EVI). The Plant Growth Index captures year-to-year variation in vegetation status, water availability, and climatic conditions. Spatially, values of the PGI are highest in tropical and subtropical regions and lowest in arid deserts. Benchmarking against gross primary productivity (GPP) from the Terrestrial Ecosystem Research Network (TERN) OzFlux network, the Normalised Difference Vegetation Index (NDVI), the Standardised Precipitation-Evapotranspiration Index (SPEI), and Australian Grassland and Rangeland Assessment by Spatial Simulation (Aussie-GRASS) indicates that PGI broadly reflects regional vegetation productivity patterns. The PGI provides a reproducible, continental-scale tool for ecological modelling, rangeland monitoring, and climate-impact studies and can be accessed at https://doi.org/10.5281/zenodo.18762343 (Retkute et al., 2026).

1 Introduction

Australia is the driest, inhabited continent, yet it spans nearly the full spectrum of global bioclimatic zones, from tropical monsoon savannas in the north to temperate woodlands, arid deserts, and alpine environments in the south (Nicholson, 2011). Only the boreal and polar climate types are absent. This diversity, combined with exceptionally high interannual variability in rainfall and temperature, makes Australia a natural laboratory for studying climatic influences on vegetation productivity. Fluctuations in productivity, driven by the El Niño–Southern Oscillation, the Indian Ocean Dipole, and the Southern Annular Mode, profoundly affect pastoral production (Cobon et al., 2019), biodiversity (Chambers et al., 2017), fire risk (Lucas et al., 2022), food-web dynamics (Letnic et al., 2005), and herbivorous insect dynamics (Wang et al., 2019). Capturing these

https://doi.org/10.5194/essd-2026-161
Preprint. Discussion started: 24 March 2026

fluctuations in a consistent and transparent way is essential for ecological research, land management, and climate-risk assessment.

Before the advent of satellite vegetation indices, early attempts to formalise growth environments relied on simple climatic scalars of light, temperature, and moisture (Fitzpatrick and Nix, 1970; 1975). These indices provided one of the first nationally consistent methods for estimating vegetation growth potential directly from climate data but relied on station observations rather than continuous gridded meteorological datasets. The indices were later incorporated into ecological simulation models, including forecasts of locust plagues (Wright, 1987). With the arrival of NASA Moderate Resolution Imaging Spectroradiometer (MODIS) and other Earth observation missions, greenness indices such as the normalized difference vegetation index (NDVI) and the enhanced vegetation index (EVI) became widely used proxies of vegetation condition, but these indices are retrospective and cannot anticipate future growth. This limitation emphasises the ongoing need for climate-driven indices that are both retrospective and forecast-aligned.

In parallel, simulation-based systems were developed for operational decision-making in the grazing sector. Most notably, Aussie-GRASS integrates Scientific Information for Land Owners (SILO) climate data, process-based pasture models, and livestock variables to support drought declaration and rangeland monitoring (Carter et al., 2000). Aussie-GRASS products, disseminated via the Long Paddock portal[1], remained the backbone of operational pasture assessment in Australia (Stone et al., 2019). More recently, the Australian Agricultural Drought Indicators (AADI) project has extended this modelling approach to deliver forward-looking, outcome-based indicators - representing aspects of agricultural outputs including crop yields, pasture growth, and farm profits - at a national scale (Hughes et al., 2025).

Here, we revisit the original scalar index framework and define a Plant Growth Index (PGI), adapted from the Pasture Growth Index (Fitzpatrick and Nix, 1975) and modernised with contemporary reanalysis and satellite-derived vegetation data. The Plant Growth Index quantifies potential vegetation growth as the product of three dimensionless scalars representing light, temperature, and moisture. Each scalar is normalised by local climatology, and the scalars are combined multiplicatively to capture joint limitation effects.

In this paper we present the first national PGI dataset. The dataset is derived using meteorology data from the Bureau of Meteorology Atmospheric high-resolution Regional Reanalysis for Australia (BARRA-R) (1990–2024, 12 km resolution) (Su et al., 2019; Wedd et al., 2022). The meteorology data are combined with maps of PFT (Harper et al. 2023), available from the ESA, and C_3/C_4 grass fractions estimated from the MODIS EVI, following Xie et al. (2022). This integration allows the index to account for regional differences in vegetation composition, particularly the distribution of C_3 versus C_4 grasses.

[1] https://www.longpaddock.qld.gov.au/

https://doi.org/10.5194/essd-2026-161
Preprint. Discussion started: 24 March 2026

Open Access Earth System Science Data Discussions

While complementary to established operational systems, the PGI emphasises reproducibility, physical consistency, and broad reuse. Since it is driven by climate variables available in both reanalysis and forecast systems, PGI provides a framework for both retrospective analysis and predictive applications, including seasonal assessment of vegetation growth potential. Its intended applications span livestock production, rangeland monitoring, biodiversity, fire ecology, and pest forecasting.The purpose of this paper is to describe the PGI dataset, including its inputs, calculation method, data records, and technical validation, to ensure transparency and support broad reuse.

2 Methodology

The Plant Growth Index (*PGI*) was quantified as the product of three biophysically relevant sub-indices: the Light Index (*LI*), Temperature Index (*TI*), and Moisture Index (*MI*). Each sub-index is standardised to a dimensionless scale ranging from 0 to 1 to ensure comparability and facilitate integration across environmental domains. The PGI was calculated as:

$$PGI(DOY, long, lat) = LI(DOY, long, lat) \times MI(DOY, long, lat) \times TI(DOY, long, lat), \quad (1)$$

where *DOY* refers to the day of year measured from the 1st of January, *long* and *lat* indicate longitude and latitude coordinates) and the multiplicative formulation captures the joint limitation effects of light availability, temperature suitability, and moisture conditions on potential plant growth. The schematic workflow for calculating the PGI from multiple environmental and vegetation datasets is shown in SI Figure S1, and details on each component are given below.

2.1 Calculation of Light Index (LI)

Hourly downward shortwave radiation data were obtained from the BARRA-R dataset, using the variable *surface_downwelling_shortwave_flux_in_air* (units: Wm^{-2}). For each grid cell, daily solar exposure (R_s, MJm^{-2}) was calculated by summing the 24hourly flux values and converting units from Wm^{-2} to $MJm^{-2}day^{-1}$:

$$R_s(DOY, lon, lat) = \sum_{h=1}^{24} SW_h(DOY, lon, lat) \times 0.036 \quad (2)$$

where SW_h is the hourly shortwave flux in Wm^{-2} and 0.0036 converts $Wm^{-2}h$ to MJ m^{-2}.

To define a location- and season-specific clear-sky reference, the clear-sky radiation baseline (R_{clear}) was computed as the 95th percentile of R_s for each day-of-year (DOY) and grid cell over the historical period 1990–2024:

$$R_{clear}(DOY, long, lat) = P_{95}\left(R_s(DOY, long, lat)\right) \quad (3)$$

The Light Index (LI) is then calculated as:

$$LI(DOY, long, lat) = min\left(1, \frac{R_s(DOY, long, lat)}{R_{clear}(DOY, long, lat)}\right) \quad (4)$$

https://doi.org/10.5194/essd-2026-161
Preprint. Discussion started: 24 March 2026

Open Access Earth System Science Data Discussions

2.2 Calculation of Moisture Index (MI)

Volumetric soil moisture data were obtained from BARRA-R (*soil_moisture*). Since the Moisture Index (MI) targets non-tree vegetation, soil moisture from the top layer (0–10 cm) was used as a proxy for root-zone moisture (θ_{rz}). For each grid cell and day-of-year (DOY), the historical 5th (P5) and 95th (P95) percentiles of θ_{rz} were computed using data from 1990–2024.

The Moisture Index was then calculated as:

$$MI(DOY, long, lat) = \min\left(1, \max\left(0, \frac{\theta_{rz}(DOY,long,lat)-P_5}{P_{95}-P_5}\right)\right) \quad (5)$$

2.3 Calculation of Temperature Index (TI)

Daily mean 2 m air temperature data were derived from BARRA-R by averaging the hourly values for each grid cell. For each tile, a normalised Brière function (Brière et al., 1999) was used to compute the Temperature Index (TI):

$$TI(DOY, long, lat) = \frac{(T(DOY,long,lat)-T_{min}^{PFT})\sqrt{T_{max}^{PFT}-T(DOY,long,lat)}}{\left(T_{opt}^{PFT}-T(DOY,long,lat)\right)\sqrt{T_{max}^{PFT}-T_{opt}^{PFT}}}, \quad (6)$$

where *TI* is calculated only for temperatures within the range $T_{min}^{PFT} \leq T \leq T_{max}^{PFT}$, for each Plant Functional Type (PFT); outside this range, $TI = 0$. Grid-level TI values were obtained by weighting tile-specific TI values by their respective PFT fractional coverage. Vegetation-specific thermal response parameters (T_{min}, T_{opt}, T_{max}) were assigned based on PFT (Table 1).

Table 1. Thermal response parameters for Plant Functional Types (PFT).

Plant Functional Types	Tmin (°C)	Topt (°C)	Tmax (°C)	Key References & Notes
C_3 Grasses (e.g. temperate native & managed pastures)	~5	18–22	~30–32	Hattersley (1983) showed C_3 dominance in regions with Jan Tmin <14–15°C. Kumarathunge et al. (2019) found canopy-scale Topt ~20°C for C_3 species; Liu et al. (2024) shows acclimation shifts of ±2–3°C seasonally.
C_4 Grasses (e.g. arid/semi-arid rangelands)	~10	28–32	~42	Hattersley (1983) and Xie et al. (2022) confirm C_4 dominance above 14–15°C Tmin. Kumarathunge et al. (2024) and Luo et al. (2024) support Topt ~30°C for C_4 canopy photosynthesis.

https://doi.org/10.5194/essd-2026-161
Preprint. Discussion started: 24 March 2026

Broad-leaved Evergreen Shrubs	~5–8	24–27	36–40	Bennett et al. (2023) and Teckentrup (2023) indicate shrubs align closer to C_3/C_4 mixed response but with mid-range Topt.
Broad-leaved Evergreen Trees	~5	22–24	~35	Kumarathunge et al. (2024) reports canopy Topt ≈ 6–8°C lower than leaf-level maxima (~30°C), consistent with Bennett et al. (2023) canopy-scale data.

We use the European Space Agency Climate Change Initiative PFT maps, which were aggregated from 300 m to 12 km resolution (Harper et al., 2023). The ESA PFT product has an annual resolution, covering 1992–2020 and indicates the specific percentage cover of the following 14 PFT-related variables: soil, built, water, snow and ice, natural grasses, managed grasses (i.e., herbaceous cropland), broad-leaved deciduous trees, broad-leaved evergreen trees, needle-leaved deciduous trees, needle-leaved evergreen trees, broad-leaved deciduous shrubs, broad- leaved evergreen shrubs, needle-leaved deciduous shrubs, and needle-leaved evergreen shrubs.

We adopted the approach of Xie et al. (2022) to classify natural grasses into C_3 and C_4 functional types. In brief, grass phenology was characterized using the MODIS Enhanced Vegetation Index (EVI) from the MYD13A1 product (Earth Science Data Systems, 2025). For each pixel and year, EVI time series were smoothed using the Whittaker filter, and phenological peaks were defined as local maxima occurring at least 128 days after the preceding peak and before the subsequent one (Retkute et al., 2024). In the Southern Hemisphere, C_4 grasses typically initiate growth in late spring to early summer, peaking in summer or autumn, whereas C_3 grasses begin in early autumn and reach their peak growth stage after winter (June-August) (Xie et al., 2022). Each 250m pixel with a single peak was classified as C_3 or C_4 grasses. Mixed C_3-C_4 grasslands exhibit two distinct growing seasons within a calendar year - the C_4 season before winter and the C_3 season after winter-resulting in two EVI peaks. In this case, we assigned a fraction to both classes according to the ratio between the two peaks. We aggregated the fractions of C_3 and C_4 grasses to a 12km grid by adding fractional coverage of 250m grid cells.

The final values for the fractional coverage of C_3 and C_4 grasses were calculated as follows:

$$f_{C3} = min(f_{C3}^{EVI} + f_{C4}^{EVI}, f_{NG}^{ESA}) \frac{f_{C3}^{EVI}}{f_{C3}^{EVI} + f_{C4}^{EVI}}, \quad (7)$$

$$f_{C4} = min(f_{C3}^{EVI} + f_{C4}^{EVI}, f_{NG}^{ESA}) \frac{f_{C4}^{EVI}}{f_{C3}^{EVI} + f_{C4}^{EVI}}. \quad (8)$$

https://doi.org/10.5194/essd-2026-161
Preprint. Discussion started: 24 March 2026

where f_{C3}^{EVI} and f_{C4}^{EVI} are C_3 and C_4 grasses fractional coverage based on EVI, and f_{NG}^{ESA} is natural grasses fractional coverage based on ESA maps.

2.4 Spatial and temporal extent and resolution.

The study was conducted across the spatial extent bounded by longitudes 113°E to 154°E and latitudes 10°S to 44°S. The temporal coverage varied depending upon each dataset used: BARRA-R reanalysis data were obtained for the period 1990–2024, ESA PFT data were available from 1992 to 2020, and land cover dynamics MODIS EVI data covered the period 2002–2024. Annual fractional coverage maps of C_3 and C_4 grasses were constructed for 2002–2020, the overlapping period between ESA PFT and MODIS EVI datasets. The 2002 fractional cover map was used to calculate the PGI for 1990–2002, and the 2020 map was used to estimate PGI for 2020–2024. The PGI maps were calculated daily for the period 1990-01-01 to 2024-12-31 at the native resolution of the BARRA-R reanalysis data (≈12 km or 0.1°).

2.5 The OzFlux Gross Primary Productivity (GPP) data

Gross Primary Productivity (GPP) data were obtained from the Terrestrial Ecosystem Research Network (TERN) OzFlux database. These data represent estimates of GPP derived from eddy covariance flux tower measurements of carbon dioxide exchange (Isaac et al., 2017). Within this system, GPP is partitioned from Net Ecosystem Exchange (NEE) using a light-response curve (LRC) method that models photosynthetic uptake and ecosystem respiration. Daily GPP values were extracted from the Level 6 (L6) PyFluxPro data release. The duration of available observations differed for each flux tower.

2.6 Australian Grassland and Rangeland Assessment by Spatial Simulation (Aussie-GRASS) data

Aussie-GRASS is based on the GRASP pasture growth model, uses a single 2009 AVHRR land-cover map, incorporates grazing and pasture-management assumptions, and is driven by the Scientific Information for Landowners climate database, SILO, (Carter et al., 2000). Data were obtained from the Long Paddock portal. We extracted the available data for the period from 1990-01-01 to 2023-12-03.

2.7 MODIS Normalised Difference Vegetation Index (NDVI) data

The MODIS/061/MYD13A1 Normalised Difference Vegetation Index (NDVI) product was used to assess vegetation dynamics and canopy greenness across the study area. The MYD13A1 dataset, derived from the Moderate Resolution Imaging Spectroradiometer (MODIS) sensor aboard NASA's Aqua satellite, provides 16-day composite NDVI data at a spatial resolution of 500 meters (Didan, 2021). For the current study, NDVI time-series data were extracted and processed using

https://doi.org/10.5194/essd-2026-161
Preprint. Discussion started: 24 March 2026

Google Earth Engine to ensure consistent temporal coverage and to minimize atmospheric or bidirectional reflectance effects. We extracted the available data for the period from 2000-02-18 to 2024-12-31.

2.8 The Standardised Precipitation-Evapotranspiration Index (SPEI) data

Meteorological drought was characterized using the Standardised Precipitation-Evapotranspiration Index (SPEI), which integrates precipitation and potential evapotranspiration to assess moisture deficits (Vicente-Serrano et al., 2010). Monthly SPEI values were obtained from the SPEI database (Beguería and Vicente-Serrano, 2023). Negative values indicate drier-than-normal periods, while positive values indicate wetter-than-normal periods. We extracted the available data for the period from 1990-01-01 till 2023-01-01 at a monthly resolution.

2.9 Pixel-wise analysis of PGI with Aussie-GRASS, NDVI, and SPEI

For each grid cell, we calculated Pearson's correlation coefficient (ρ) between corresponding values of Aussie-GRASS, NDVI, and SPEI. For the correlation between PGI and Aussie-GRASS, values were aligned on the same day. Because the temporal resolution of NDVI and SPEI is coarser, and these variables reflect accumulated rather than instantaneous responses to meteorological conditions, we introduced a time lag (l), such that the correlation was calculated between NDVI/SPEI values at day d and PGI values at day ($d - l$). We then retained the maximum correlation value for $l \in [0, 30]$ days.

2.10 The Interim Biogeographic Regionalisation for Australia (IBRA)

The study area was delineated using the Interim Biogeographic Regionalisation for Australia, version 7 (IBRA7), in which Australia is divided into 89 bioregions based on shared climate, geology, landform, native vegetation, and species characteristics (Thackway and Cresswell, 1995). Spatial boundaries and land-unit attributes were accessed through the Australian Government's data catalogue (Department of Climate Change, Energy, the Environment and Water, 2022). Four bioregions (*Coral Sea*, *Indian Tropical Islands*, *Pacific Subtropical Islands*, and *Subantarctic Islands*) were excluded from the analysis because they represent offshore island or marine bioregions.

3 Results

3.1 Characteristics of PGI

Country-wide daily mean PGI ranged from 0.01 to 0.28 for the years 1990-2024. Temporal patterns of PGI, including the mean, 25–75% quantiles, and 5-95% quantiles, are shown in Figure 1a. We extracted periods during which the mean PGI was

https://doi.org/10.5194/essd-2026-161
Preprint. Discussion started: 24 March 2026

Open Access Earth System Science Data Discussions

sustained at low levels (lower quartile) or high levels (upper quartile) for at least 30 days. There were 14 periods of sustained low PGI and 16 periods of sustained high PGI. The longest sustained low-PGI period lasted almost 200 days (April–October 1994), followed by a 119-day period in May–August 2002. Two periods of sustained high PGI lasted approximately 100 days, occurring in February–May 2000 and February–May 2011. The spatial distribution of PGI on the date with the lowest mean PGI (30 June 2002) is presented in Figure 1b. More than half of the area (56%) had PGI values below 0.01. In contrast, Figure 1c shows PGI values on the date of highest mean PGI (22 March 2011), where 20% of area had PGI values above 0.5.

Pixel-wise mean PGI varied considerably across Australia's IBRA7 bioregions (Fig. 1d). The highest mean PGI values were observed in the Wet Tropics (0.317), Pine Creek (0.312), and Daly Basin (0.309), indicating consistently high potential growth in these tropical and subtropical regions. Other regions with relatively high mean PGI included Darwin Coastal (0.279), Central Arnhem (0.276), and Cape York Peninsula (0.259). As expected, the lowest mean PGI values were found in arid and desert regions, exemplified by the Simpson Strzelecki Dunefields (0.015), Broken Hill Complex (0.032), Davenport Murchison Ranges (0.036), Tanami Desert (0.036) and Stony Plains (0.036). Intermediate values were observed in temperate and semi-arid regions, such as Tasmanian West (0.215), Southeastern Queensland (0.221), and NSW North Coast (0.254). Overall, the distribution of mean PGI highlights a clear gradient from high potential growth in tropical and coastal regions to low potential growth in arid interior and desert regions, reflecting the strong influence of climate and environmental conditions on vegetation productivity across Australia.

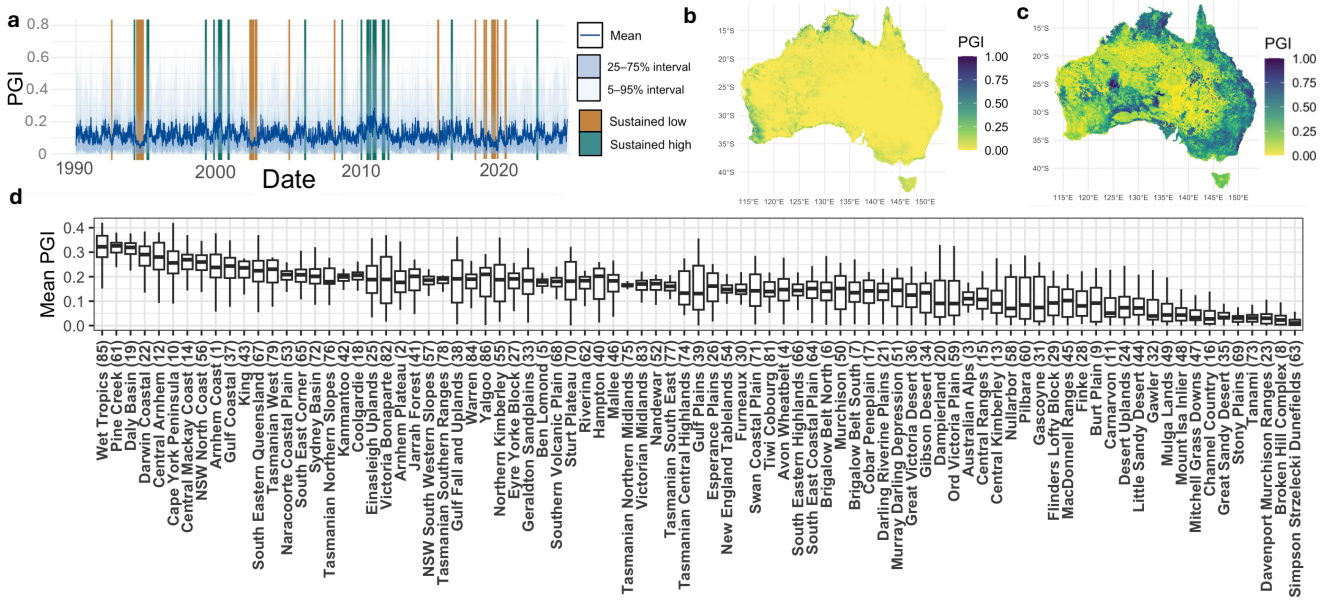

Figure 1. (a) Mean PGI from 1990 to 2024 with 25–75% (dark shading) and 5–95% (light shading) quantiles. The background highlights time periods during which the mean PGI was sustained at low levels (lower quartile) or high levels (upper quartile) for at least 30 days. (b)

https://doi.org/10.5194/essd-2026-161
Preprint. Discussion started: 24 March 2026

Spatial PGI distribution on 2002-06-30. (c) PGI values on 2011-03-22. (d) Distribution of the pixel-wise (0.1° resolution) mean PGI from 1990 to 2024 aggregated at the IBRA7 bioregions scale. Numbers next to each bioregion in (d) correspond to the labels on the map in Fig.3(d).

3.2 Benchmarking PGI against GPP

We evaluated the relationship between the PGI and GPP using daily time series data from 27 flux tower sites distributed across major Australian biomes (Figure 2, SI Figure S2). The correlations between PGI and GPP were consistently positive, ranging from $\rho = 0.08$ to $\rho = 0.94$,with a median of $\rho = 0.66$ (Figure 2a). The strongest relationships were observed in cooler and temperate biomes with clear seasonal cycles, including the Alpine Peatland ($\rho = 0.94$), Fletcherview (Desert Uplands; $\rho = 0.90$), and Longreach (Mitchell Grass Downs; $\rho = 0.76$) (Figure 2b), where PGI effectively reflected the meteorological conditions underpinning vegetation functioning. Similarly, strong correlations in tropical savanna sites such as Howard Springs ($\rho = 0.70$) and Litchfield ($\rho = 0.69$) (Figure 2b) indicate that PGI effectively captures productivity responses to wet–dry season transitions. Weak to moderate correlations were found in coastal and semi-arid ecosystems such as the Wet Tropics ($\rho = 0.12$–0.25), Avon Wheatbelt ($\rho = 0.27$–0.66), and South East Coastal Plain ($\rho = 0.38$) (SI Figure S2), where local canopy or soil moisture dynamics may decouple potential and realized productivity.

https://doi.org/10.5194/essd-2026-161
Preprint. Discussion started: 24 March 2026

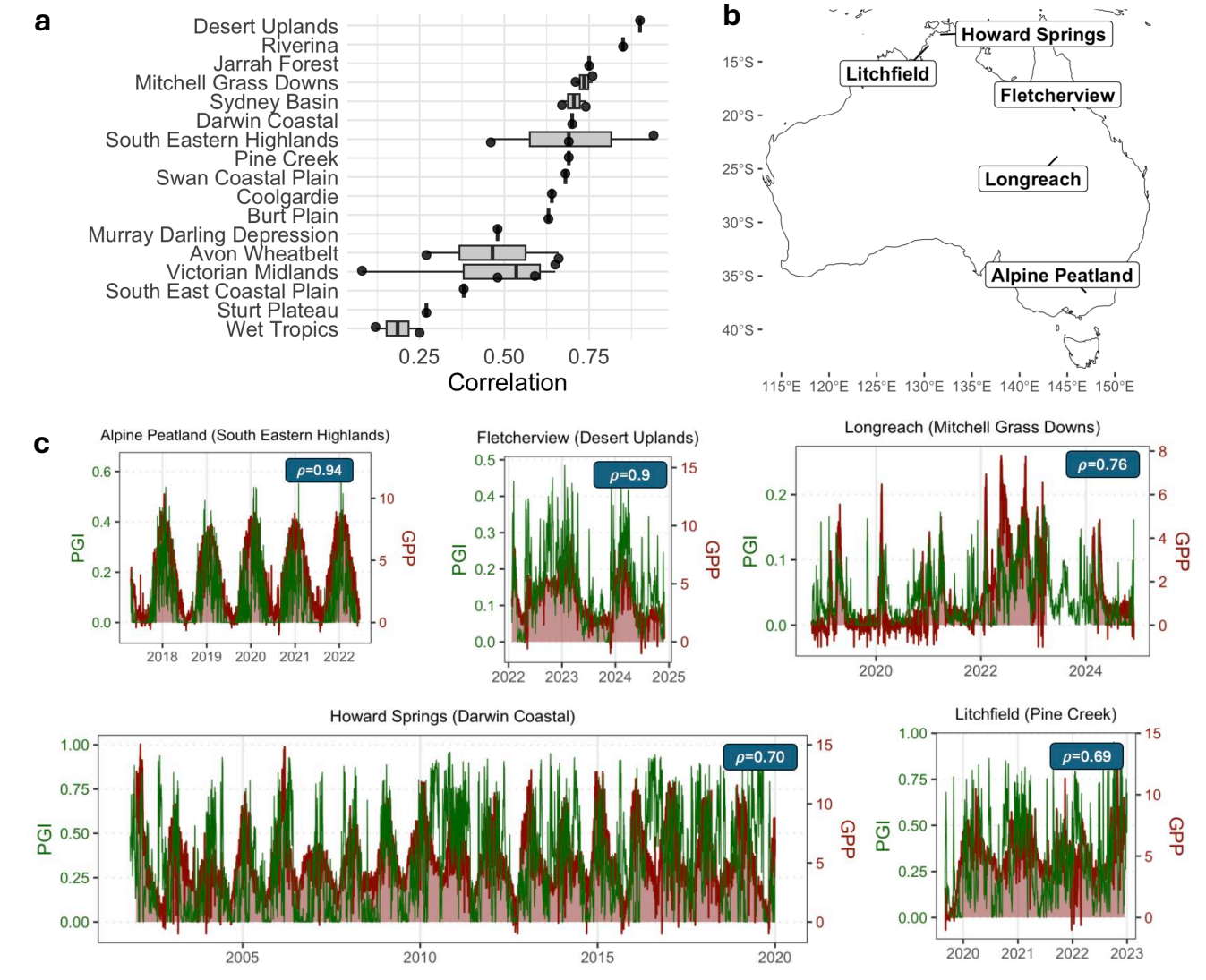

Figure 2. Benchmarking PGI against GPP. (a) Distribution of correlation coefficients in decreasing order between Plant Growth Index (PGI) and Gross Primary Productivity (GPP) as a function of subset of IBRA7 bioregion containing flux towers. (b-c) Location of flux towers and relationship between PGI and GPP for selected sites. Daily values of the Plant Growth Index (PGI) (green line, right y-axis) are plotted together with GPP (red line and pink filled area, left y-axis) for the same period. The name of each flux tower and its corresponding IBRA7 bioregion are shown above each panel. The correlation coefficient between smoothed values is displayed in the blue box. (See SI Fig. 2 for the full set of available sites).

https://doi.org/10.5194/essd-2026-161
Preprint. Discussion started: 24 March 2026

Open Access Earth System Science Data Discussions

3.3 Comparison of PGI with Aussie-GRASS, NDVI, and SPEI

PGI-Aussie-GRASS correlation was calculated over 33 years of daily data, the PGI–SPEI correlation over 33 years of monthly data, and the PGI–NDVI correlation over five years of bi-weekly data (Fig. 3a-c). The strongest overall relationship was observed between PGI and Aussie-GRASS (median = 0.48; range = (-0.2; 0.83), followed by PGI–SPEI (median = 0.46; range = (-0.3; 0.8)) and PGI–NDVI (median = 0.40; range = (–0.07;0.60)). Across the all Australian IBRA7 bioregions, pixel-wise correlations between the Plant Growth Index (PGI) and three reference datasets (Aussie-GRASS, NDVI, and SPEI) were generally positive but varied widely among regions (Fig. 3d-f). Strong correlations with Aussie-GRASS occurred in mesic and high-altitude regions such as the Australian Alps (median = 0.75), New England Tablelands (median = 0.72), and South Eastern Highlands (median = 0.71). Correlations were moderate in southwestern semi-arid regions, including the Esperance Plains (median = 0.41), and forested regions (Jarrah Forest median = 0.26), where local environmental constraints may weaken agreement between different estimates of potential growth. Strong PGI–NDVI correlations were found in arid and savanna biomes such as the Brigalow Belt North (median = 0.62), Finke (median = 0.62), and Simpson–Strzelecki Dunefields (median = 0.63), suggesting that PGI effectively captures spatial variation in greenness across water-limited systems. Similarly, moderate PGI–SPEI correlations across most biomes indicate that potential growth is broadly consistent with patterns of moisture availability, with the strongest coupling in rangeland and desert systems such as the Desert Uplands (median = 0.51) and Mulga Lands (median = 0.48).

https://doi.org/10.5194/essd-2026-161
Preprint. Discussion started: 24 March 2026

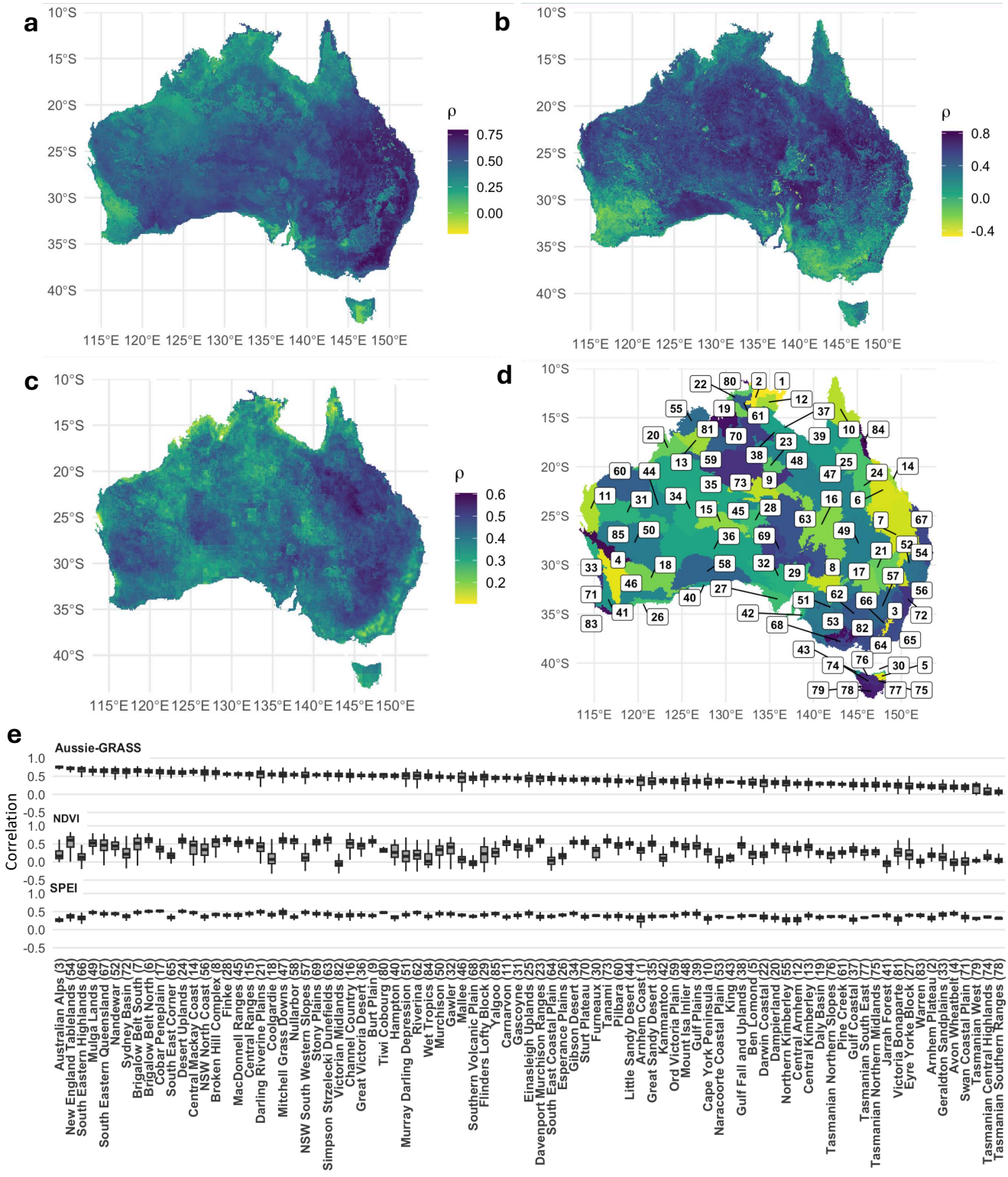

https://doi.org/10.5194/essd-2026-161
Preprint. Discussion started: 24 March 2026

Figure 3. Distribution of pixel-wise correlation. (a) Correlation between PGI and Aussie-GRASS. (b) Correlation between PGI and NDVI. (c) Correlation between PGI and SPEI. (d) Map showing IBRA7 bioregions. (e) Distribution of correlations between PGI and Aussie-GRASS/NDVI/SPEI for IBRA7 bioregion. Numbers on the map in (d) correspond to bioregions next to a number in (e).

4 Discussion

This study presents the first national Plant Growth Index dataset for Australia (1990–2024), integrating gridded meteorological reanalysis, satellite-derived vegetation fractional cover, and plant functional type information. The PGI is designed as a data product that quantifies potential vegetation growth across climate, moisture, and light gradients in a unified, reproducible framework with daily temporal resolution at ~0.1° spatial resolution. By explicitly incorporating PFTs and vegetation fractional coverage, the PGI advances beyond legacy climate scalars and greenness proxies by capturing how vegetation composition interacts with climate drivers to shape potential growth. This key attribute distinguishes the PGI from earlier scalar indices that relied on station data alone and from retrospective greenness indices that lack explicit vegetation composition information.

Our analysis of the PGI across Australia highlights strong spatial and temporal variability in potential vegetation growth, reflecting the influence of climate, soil, and hydrological conditions. PGI was generally highest in tropical and subtropical high-rainfall regions, lowest in arid zones, and intermediate in temperate and semi-arid areas, consistent with continental-scale ecohydrological gradients (Paudel et al., 2025). Country-wide daily mean PGI ranged from 0.01 to 0.28, with extended low- or high-PGI periods reflecting persistent environmental constraints or favourable conditions. The longest low-PGI spell (~200 days, April–October 1994) coincided with severe drought in New South Wales, causing ~5 billion AUD in losses (Australian Institute for Disaster Resilience, 1994), whereas a high-PGI period (~100 days, February–May 2011) aligned with the strong 2010–11 La Niña (Boening et al., 2013). Comparisons with flux-tower GPP (OzFlux), MODIS NDVI, Aussie-GRASS, and SPEI indicate that PGI broadly captures patterns of vegetation growth and moisture availability, with strongest agreement in temperate and tropical savanna regions and weaker correlations in coastal, semi-arid, and forested areas, where local canopy structure, soil heterogeneity, or fine-scale hydrology may decouple potential from realized productivity (De Pue et al., 2023).

The use of remote sensing and reanalysis data confers substantial advantages for the PGI. Unlike data products based solely on in-situ networks or static land cover maps, the PGI draws on continuous gridded inputs that reflect both climatic variability and vegetation structure, enabling consistent spatiotemporal mapping over broad regions and long time periods. In doing so, it addresses common limitations of older growth indices that lacked geographically consistent, high-resolution inputs and is immediately compatible with widely used Earth observation datasets. The PGI dataset thus supports cross-regional comparison and integration with other gridded data sources in Earth system research.

https://doi.org/10.5194/essd-2026-161
Preprint. Discussion started: 24 March 2026

The contemporary daily resolution of the PGI data product, spanning more than three decades, enables users to characterise interannual variability, seasonal cycles, and responses to extreme climate events such as droughts and La Niña phases. This feature makes PGI suitable for a range of applications, including ecological monitoring, drought and fire risk assessment, and as a baseline for evaluating climate impacts or model simulations. Since PGI is driven by large-scale climate variables and vegetation structure, it is naturally suited to sub-seasonal and seasonal forecasting applications using existing climate prediction systems. This enables forward-looking assessments of vegetation growth potential that complement retrospective indicators such as NDVI, supporting operational planning in rangeland management, biosecurity, and climate-risk assessment.

At the continental scale, mean PGI broadly follows rainfall variability, reflecting the dominant role of moisture availability in regulating vegetation growth potential (Donohue et al., 2009; Piao et al., 2020). However, deviations from this relationship arise in habitats with intrinsically sparse vegetation cover, such as the Stony Plains, which typically exhibit lower PGI values than more densely vegetated systems such as the Mitchell Grass Downs. This difference reflects not only lower median rainfall but also reduced vegetation cover and productivity potential in these environments. Sparse vegetation and exposed substrate can limit detectable greenness in satellite-derived indices, particularly in earlier remote sensing products (Fensholt and Proud, 2012), whereas the climate-driven PGI framework provides a more consistent representation of underlying growth potential. These differences highlight the importance of considering both climatic forcing and vegetation structure when interpreting spatial variation in PGI.

Many fine-scale processes that influence vegetation growth are not captured at the ~12 km resolution of the PGI. For example, runoff from stone-covered surfaces can redistribute water into adjacent grass-dominated areas, particularly along drainage lines where moisture accumulates and supports greater vegetation density. These localised hydrological processes can enable rapid and sustained grass growth following relatively small rainfall events (Hunter and Melville, 1994), even in landscapes that are otherwise sparsely vegetated. Similarly, local disturbances such as grazing can substantially alter vegetation structure and productivity at spatial scales smaller than the PGI grid (Moore et al., 2015). Consequently, while PGI provides consistent estimates of average climate-driven growth potential across broad bioregions, it necessarily smooths over fine-scale heterogeneity arising from local hydrology, vegetation structure, and land use, and these factors should be considered when applying PGI to site-specific ecological or management questions. The PGI data product complements existing remote sensing and ecosystem datasets in the Earth system sciences by offering a reproducible, and climate-centric view of potential vegetation growth that can be readily reused by the community. Its broad coverage and methodological transparency support integration with other Earth system datasets, model benchmarking, and long-term ecological studies requiring consistent baseline data. Future work may extend the data product by incorporating updated vegetation maps or forecasting capabilities using seasonal climate predictions, further enhancing the PGI's utility for operational planning, climate risk assessment, and interdisciplinary research. Such capabilities are particularly relevant for herbivore forecasting applications such as locust early warning, where

https://doi.org/10.5194/essd-2026-161
Preprint. Discussion started: 24 March 2026

climate-driven vegetation growth plays a central role in determining survival, reproduction, and migration dynamics (Wang et al., 2019; Mangeon et al., 2020; Lawton et al., 2022; Retkute et al., 2024).

5 Data availability

The Plant Growth Index (PGI) dataset is publicly available via the Zenodo repository at https://doi.org/10.5281/zenodo.18762343 (Retkute et al., 2026A). The dataset includes daily gridded PGI values for Australia at ~12 km resolution for the period 1990–2024, provided in NetCDF format. The repository contains all data and metadata required to reproduce the analyses presented in this study. The code for calculating and mapping the Plant Growth Index is publicly available on GitHub (Retkute, 2026B).

Financial support

This work was supported in part by the Gates Foundation INV070408 (CAG and RR). RR acknowledges support through an award from the BBSRC Flexible Talent Mobility Account.

Author contribution

RR, AS, DH, and CAG conceived the study. AS & RR jointly developed the methodology. RR performed the analyses and wrote the first draft of the manuscript. All authors analysed the results and contributed to the manuscript.

Competing interests

The authors declare that they have no competing interests.

https://doi.org/10.5194/essd-2026-161
Preprint. Discussion started: 24 March 2026

Appendix A

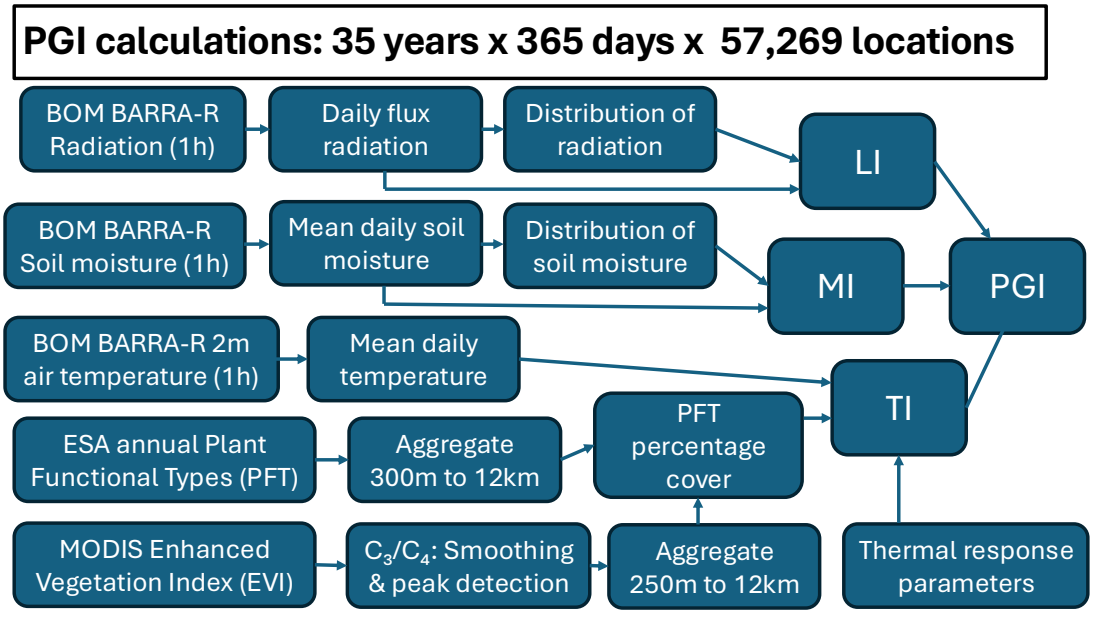

Figure A1. Schematic workflow for calculating the Plant Growth Index (PGI) from multiple environmental and vegetation datasets. Hourly radiation, soil moisture, and 2 m air temperature from BOM BARRA-R are processed to obtain daily fluxes and distributions, which are used to compute the Light Index (LI), Moisture Index (MI), and Temperature Index (TI). Distributions are calculated for each 12 km grid cell and day-of-year. ESA annual Plant Functional Types (PFT) and MODIS Enhanced Vegetation Index (EVI) are aggregated to derive PFT percentage cover and vegetation activity, which feed into the TI calculation. Thermal response parameters are incorporated in the TI derivation. The LI, MI, and TI are then combined to generate the PGI.

https://doi.org/10.5194/essd-2026-161
Preprint. Discussion started: 24 March 2026

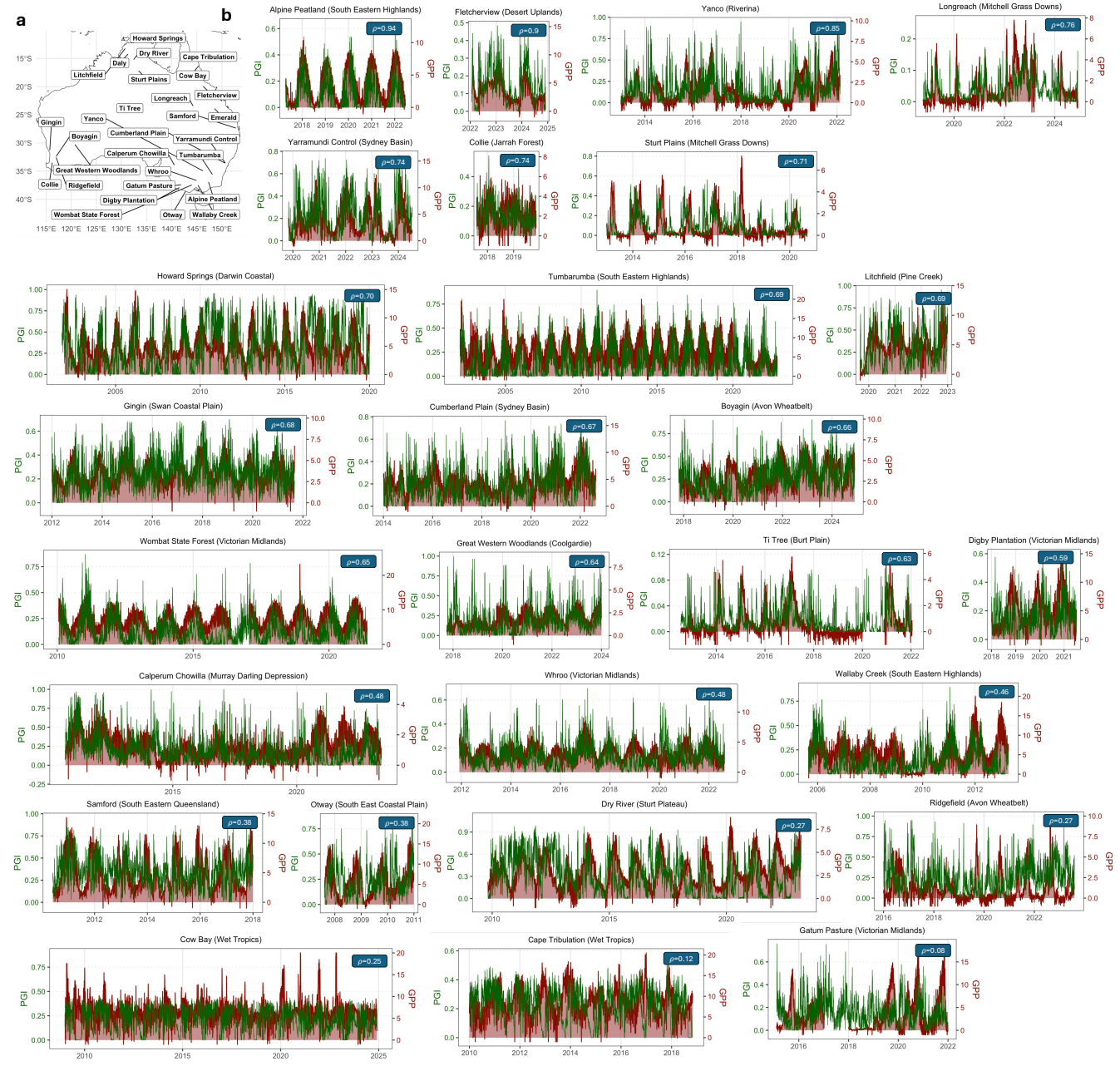

Figure A2. Benchmarking PGI against GPP. (a) Location of flux towers. (b) Daily values of the Plant Growth Index (PGI) (green line, right y-axis) are plotted together with Gross Primary Productivity (GPP) (red line and pink filled area, left y-axis) for the same period. The name of each flux tower and its corresponding IBRA7 bioregion are shown above each panel. The correlation between smoothed values is displayed in the blue box.

https://doi.org/10.5194/essd-2026-161
Preprint. Discussion started: 24 March 2026

References

ABARES. (2022). *The Drought Early Warning System (DEWS) Project* (ABARES Research Report 22.13). ABARES, Canberra. https://doi.org/10.25814/2nd3-em96

Australian Institute for Disaster Resilience. (1994). *Severe drought in eastern and northern Australia*. https://knowledge.aidr.org.au/resources/environment-severe-drought-eastern-and-northern-australia/

Beguería, S., Vicente-Serrano, S.M. (2023). SPEIbase v2.9 [Data set]. DIGITAL.CSIC. https://doi.org/10.20350/digitalCSIC/15470

Bennett, A. C., Knauer, J., Bennett, L. T., Haverd, V., & Arndt, S. K. (2024). Variable influence of photosynthetic thermal acclimation on future carbon uptake in Australian wooded ecosystems under climate change. *Global Change Biology*, *30*(1), e17021. https://doi.org/10.1111/gcb.17021

Brière, J.-F., Pracros, P., Le Roux, A.-Y., & Pierre, J.-S. (1999). A novel rate model of temperature-dependent development for arthropods. *Environmental Entomology*, 28(1), 22–29. https://doi.org/10.1093/ee/28.1.22

Boening, C., Willis, J. K., Landerer, F. W., Nerem, R. S., & Fasullo, J. (2012). The 2011 La Niña: So strong, the oceans fell. *Geophysical Research Letters*, *39*(19). https://doi.org/10.1029/2012GL053055

Carter, J. O., Hall, W. B., Brook, K. D., McKeon, G. M., Day, K. A., & Paull, C. J. (2000). Aussie-GRASS: Australian grassland and rangeland assessment by spatial simulation. In G. L. Hammer, N. Nicholls, & C. Mitchell (Eds.), *Applications of seasonal climate forecasting in agricultural and natural ecosystems: The Australian experience* (pp. 329–349). Kluwer Academic Publishers. http://link.springer.com/chapter/10.1007/978-94-015-9351-9_20

Chambers, L. E., Barnard, P., Poloczanska, E. S., Hobday, A. J., Keatley, M. R., Allsopp, N., & Underhill, L. G. (2017). Southern hemisphere biodiversity and global change: data gaps and strategies. *Austral Ecology*, *42*(1), 20-30. https://doi.org/10.1111/aec.12391

Cobon, D. H., Kouadio, L., Mushtaq, S., Jarvis, C., Carter, J., Stone, G., & Davis, P. (2019). Evaluating the shifts in rainfall and pasture-growth variabilities across the pastoral zone of Australia during 1910–2010. *Crop and Pasture Science*, *70*(7), 634-647. https://doi.org/10.1071/CP18482

https://doi.org/10.5194/essd-2026-161
Preprint. Discussion started: 24 March 2026

Department of Climate Change, Energy, the Environment and Water. (2022). *Interim Biogeographic Regionalisation for Australia (IBRA), Version 7 – Regions* [Data set]. Australian Government. https://data.gov.au/data/dataset/d44dd392-ebea-4f1a-b30e-4a2da154aae4

De Pue, J., Wieneke, S., Bastos, A., Barrios, J. M., Liu, L., Ciais, P., ... & Balzarolo, M. (2023). Temporal variability of observed and simulated gross primary productivity, modulated by vegetation state and hydrometeorological drivers. *Biogeosciences*, *20*(23), 4795-4818. https://doi.org/10.5194/bg-20-4795-2023

Didan, K. (2021). *MOD13A1 MODIS/Terra Vegetation Indices 16-Day L3 Global 500m SIN Grid V061*. NASA EOSDIS Land Processes DAAC. https://doi.org/10.5067/MODIS/MOD13A1.061

Donohue, R. J., McVICAR, T. R., & Roderick, M. L. (2009). Climate-related trends in Australian vegetation cover as inferred from satellite observations, 1981–2006. *Global Change Biology*, *15*(4), 1025-1039. https://doi.org/10.1111/j.1365-2486.2008.01746.x

Earth Science Data Systems. (2025). *MODIS/Terra Vegetation Indices 16-Day L3 Global 500m SIN Grid V006*. NASA Earthdata. https://doi.org/10.5067/MODIS/MOD13A1.061

Fitzpatrick, E. A., & Nix, H. A. (1970). The climatic factor in Australian grasslands ecology. In R. M. Moore (Ed.), *Australian Grasslands* (pp. 3–26). Australian National University Press.

Fitzpatrick, E. A., & Nix, H. A. (1975). *The Climatic Index of Pasture Growth*. CSIRO.**Fensholt, R. and Proud, S. R.:** Evaluation of Earth observation based global long-term vegetation trends – Comparing GIMMS and MODIS global NDVI time series, *Remote Sensing of Environment*, **119**, 131–147, https://doi.org/10.1016/j.rse.2011.12.015, 2012.

Harper, K. L., Lamarche, C., Hartley, A., Peylin, P., Ottlé, C., Bastrikov, V., San Martín, R., Bohnenstengel, S. I., Kirches, G., Boettcher, M., Shevchuk, R., Brockmann, C., & Defourny, P. (2023). A 29-year time series of annual 300 m resolution plant-functional-type maps for climate models. *Earth System Science Data, 15*(3), 1465–1499. https://doi.org/10.5194/essd-15-1465-2023

Hughes, N., Gaydon, D., Gupta, M., Schepen, A., Tan, P., Brent, G., Turner, A., Bellew, S., Soh, W. Y., Sharman, C., Taylor, P., Carter, J., Bruget, D., Hochman, Z., Searle, R., Song, Y., Mitchell, P., Beletse, Y., Holzworth, D., Guillory, L., … Singh, R. (2025). Monitoring agricultural and economic drought: The Australian Agricultural Drought Indicators (AADI). *Natural Hazards and Earth System Sciences, 25*, 3461–3482. https://doi.org/10.5194/nhess-25-3461-2025

https://doi.org/10.5194/essd-2026-161
Preprint. Discussion started: 24 March 2026

Hunter, D.M. and Melville, M. D. (1994). The rapid and long-lasting growth of grasses following small falls of rain in the arid interior of Australia. *Aust. J. Ecol.* 19: 46-51. https://doi.org/10.1111/j.1442-9993.1994.tb01542.x

Hattersley, P. W. (1983). *The distribution of C_3 and C_4 grasses in Australia in relation to climate*. *Oecologia*, 57(1–2), 113–128. https://doi.org/10.2307/4216935

Isaac, P., Cleverly, J., McHugh, I., van Gorsel, E., Ewenz, C., and Beringer, J. (2017) OzFlux data: network integration from collection to curation, *Biogeosciences*, 14, 2903–2928, https://doi.org/10.5194/bg-14-2903-2017

Kumarathunge, D. P., Medlyn, B. E., Drake, J. E., Tjoelker, M. G., Aspinwall,M. J., Battaglia, M., Cano, F. J., Carter, K. R., Cavaleri, M. A.,Cernusak, L. A., Chambers, J. Q., Crous, K. Y., De Kauwe, M. G.,Dillaway, D. N., Dreyer, E., Ellsworth, D. S., Ghannoum, O., Han, Q.,Hikosaka, K.,…Way, D. A. (2019). Acclimation and adaptationcomponents of the temperature dependence of plant photosynthesis atthe global scale.New Phytologist,222(2), 768-784. https://doi.org/https://doi.org/10.1111/nph.15668

Kumarathunge, D. P., Medlyn, B. E., Drake, J. E., De Kauwe, M. G., Tjoelker, M. G., Aspinwall, M. J., … Crous, K. Y. (2024). Photosynthetic temperature responses in leaves and canopies: why temperature optima may disagree at different scales. Tree Physiology, 44(11), tpae135. https://doi.org/10.1093/treephys/tpae135

Lawton, D., Scarth, P., Deveson, E., Piou, C., Spessa, A., Waters, C., & Cease, A. J. (2022). Seeing the locust in the swarm: accounting for spatiotemporal hierarchy improves ecological models of insect populations. *Ecography*, *2022*(2). https://doi.org/10.1111/ecog.05763

Letnic, M., Tamayo, B., & Dickman, C. R. (2005). The responses of mammals to La Nina (El Nino Southern Oscillation)–associated rainfall, predation, and wildfire in central Australia. *Journal of mammalogy*, *86*(4), 689-703. https://doi.org/10.1644/1545-1542(2005)086[0689:TROMTL]2.0.CO;2

Liu, J., Ryu, Y., Luo, X., Dechant, B., Stocker, B. D., Keenan, T. F., … Prentice, I. C. (2024). Evidence for widespread thermal acclimation of canopy photosynthesis. Nature Plants, 10(12), 1919–1927. https://doi.org/10.1038/s41477-024-01846-1

Lucas, C., Dowdy, A. J., & Fogarty, L. (2022). Climate drivers of potential fire intensity in Australia: The role of ENSO, IOD, and SAM. International Journal of Wildland Fire, 31(6), 567–582. https://doi.org/10.1071/WF2306

https://doi.org/10.5194/essd-2026-161
Preprint. Discussion started: 24 March 2026

Luo, X., Zhou, H., Satriawan, T. W., Tian, J., Zhao, R., Keenan, T. F., ... & Still, C. J. (2024). Mapping the global distribution of C4 vegetation using observations and optimality theory. *Nature Communications*, *15*(1), 1219. https://doi.org/10.1038/s41467-024-45606-3

Mangeon, S., Spessa, A., Deveson, E. *et al.* Daily mapping of Australian Plague Locust abundance. *Sci Rep* **10**, 16915 (2020). https://doi.org/10.1038/s41598-020-73897-1

Moore, E. K., Britton, A. J., Iason, G., Pemberton, J., and Pakeman, R. J. (2015). Landscape-scale vegetation patterns influence small-scale grazing impacts. *Biological Conservation*, *192*, 218-225. https://doi.org/10.1016/j.biocon.2015.09.019

Nicholson SE. (2011) Australia. In: *Dryland Climatology*. Cambridge University Press:337-350.

Paudel, P., Olin, S., Tjoelker, M., Pontarp, M., Metcalfe, D., & Smith, B. (2025). Savanna ecosystem structure and productivity along a rainfall gradient: the role of competition and stress tolerance mediated by plant functional traits. *Biogeosciences*, *22*(20), 6153-6171. https://doi.org/10.5194/bg-22-6153-2025

Piao, S., Wang, X., Park, T., Chen, C., Lian, X. U., He, Y., ... & Myneni, R. B. (2020). Characteristics, drivers and feedbacks of global greening. *Nature Reviews Earth & Environment*, *1*(1), 14-27. https://doi.org/10.1038/s43017-019-0001-x

Retkute, R., Thurston, W., Cressman, K., & Gilligan, C. A. (2024). A framework for modelling desert locust population dynamics and large-scale dispersal. *PLOS Computational Biology, 20*(3), e1012562. https://doi.org/10.1371/journal.pcbi.1012562

Retkute, R., Spessa, A., Hunter, D., & Gilligan, C. (2026A). Mapping Plant Growth Index (PGI) over Australia from 1990 to 2024 (Version v1) [Data set]. Zenodo. https://doi.org/10.5281/zenodo.18762343

Retkute, R. (2026B) *Mapping-Plant-Growth-Index* [Computer software]. https://github.com/rretkute/Mapping-Plant-Growth-Index

Stone G., Pozza R.D., Carter J., & McKeon G. (2019) Long Paddock: climate risk and grazing information for Australian rangelands and grazing communities. *The Rangeland Journal* 41, 225–232. https://doi.org/10.1071/RJ18036

Su, C.-H., Eizenberg, N., Steinle, P., Jakob, D., Fox-Hughes, P., White, C.J., Rennie, S., Franklin, C., Dharssi, I., & Zhu, H. (2019). *BARRA v1.0: the Bureau of Meteorology Atmospheric high-resolution Regional Reanalysis for Australia*. Geosci. Model Dev., 12, 2049–2068. https://doi.org/10.5194/gmd-12-2049-2019

https://doi.org/10.5194/essd-2026-161
Preprint. Discussion started: 24 March 2026

Teckentrup, L., De Kauwe, M. G., Abramowitz, G., Pitman, A. J., Ukkola, A. M., Hobeichi, S., ... & Smith, B. (2023). *Opening Pandora's box: reducing global circulation model uncertainty in Australian simulations of the carbon cycle, Earth Syst. Dynam., 14, 549–576*. https://doi.org/10.5194/esd-14-549-2023

Thackway, R., & Cresswell, I. D. (1995). *An interim biogeographic regionalisation for Australia: A framework for setting priorities in the National Reserves System Cooperative Program* (Version 4.0, updated). Australian Nature Conservation Agency, Canberra.

Vicente-Serrano, S. M., Beguería, S., López-Moreno, J. I., Angulo, M., & El Kenawy, A. (2010). A multiscalar drought index sensitive to global warming: The Standardized Precipitation-Evapotranspiration Index (SPEI). Journal of Climate, 23(7), 1696–1718. https://doi.org/10.1175/2009JCLI2909.1

Wedd, R., Alves, O., de Burgh-Day, C., Down, C., Griffiths, M., Hendon, H. H., ... & Zhou, X. (2022). ACCESS-S2: the upgraded Bureau of Meteorology multi-week to seasonal prediction system. *Journal of Southern Hemisphere Earth Systems Science*, *72*(3), 218-242. ACCESS-S2: The upgraded Bureau of Meteorology multi-week to seasonal prediction system. *Quarterly Journal of the Royal Meteorological Society, 149*(755), 2260–2289. https://doi.org/10.1002/qj.4550

Wang, B., Deveson, E. D., Waters, C., Spessa, A., Lawton, D., Feng, P., & Liu, D. L. (2019). Future climate change likely to reduce the Australian plague locust (Chortoicetes terminifera) seasonal outbreaks. Science of the Total Environment, 668, 947–957. https://doi.org/10.1016/j.scitotenv.2019.02.439

Wright, D. E. (1987). A simulation model of plague dynamics in the Australian plague locust (*Chortoicetes terminifera*). *Australian Journal of Ecology, 12*(4), 423–437. https://doi.org/10.1111/j.1442-9993.1987.tb00958.x

Xie, Q., Huete, A., Hall, C. C., Medlyn, B. E., Power, S. A., Davies, J. M., Medek, D. E., & Beggs, P. J. (2022). Satellite-observed shifts in C_3/C_4 abundance in Australian grasslands are associated with rainfall patterns. *Remote Sensing of Environment, 273*, 112983. https://doi.org/10.1016/j.rse.2022.112983